



**CHALMERS**  
UNIVERSITY OF TECHNOLOGY

## **The Influence of KCl and HCl on the High-Temperature Oxidation of a Fe-2.25Cr-1Mo Steel at 400 °C**

Downloaded from: <https://research.chalmers.se>, 2023-05-05 06:34 UTC

Citation for the original published paper (version of record):

Larsson, E., Liske, J., Persdotter, A. et al (2020). The Influence of KCl and HCl on the High-Temperature Oxidation of a Fe-2.25Cr-1Mo Steel at 400 °C. *Oxidation of Metals*, 93(1-2): 29-52. <http://dx.doi.org/10.1007/s11085-019-09943-9>

N.B. When citing this work, cite the original published paper.



# The Influence of KCl and HCl on the High-Temperature Oxidation of a Fe-2.25Cr-1Mo Steel at 400 °C

E. Larsson<sup>1</sup> · J. Liske<sup>1</sup> · A. Persdotter<sup>1</sup> · T. Jonsson<sup>1</sup> · J. -E. Svensson<sup>1</sup> · L. -G. Johansson<sup>1</sup>

Received: 23 August 2019 / Revised: 31 October 2019  
© The Author(s) 2019

## Abstract

The influence of alkali- and chlorine-containing compounds on the corrosion of superheater alloys has been studied extensively. The current paper instead investigates the corrosive effects of KCl and HCl under conditions relevant to waterwall conditions. A low-alloy (Fe-2.25Cr-1Mo) steel was exposed to KCl(s), 500 vppm HCl(g) and (KCl+HCl) in the presence of 5% O<sub>2</sub> and 20% H<sub>2</sub>O at 400 °C. The results indicate that alloy chlorination by KCl occurs by an electrochemical process, involving cathodic formation of chemisorbed KOH on the scale surface and anodic formation of solid FeCl<sub>2</sub> at the bottom of the scale. The process is accompanied by extensive cracking and delamination of the iron oxide scale, resulting in a complex, convoluted scale morphology. Adding 500 vppm HCl to the experimental environment (KCl+HCl) initially greatly accelerated the formation of FeCl<sub>2</sub> at the scale/alloy interface. The accelerated alloy chlorination is attributed to HCl reacting with KOH at the scale surface, causing the cathodic process to be depolarized. A rapid slowing down of the rate of chlorination and corrosion in KCl+HCl environment was observed which was attributed to the electronically insulating nature of the FeCl<sub>2</sub> layer which forms at the bottom of the scale, disconnecting the anodic and cathodic regions.

**Keywords** KCl · HCl · Chlorine-induced corrosion · Waterwalls · Low-alloyed steel · Corrosion mechanism

---

✉ J. Liske  
jesper.liske@chalmers.se

<sup>1</sup> Environmental Inorganic Chemistry, Department of Chemistry and Chemical Engineering, Chalmers University of Technology, 412 96, Göteborg, Sweden

## Introduction

To raise power production from biomass- and waste-fired boilers, it is necessary to increase the steam data of the plants and hence the temperature of both the steam superheaters and the waterwalls. However, higher material temperatures tend to be accompanied by increased fireside corrosion, causing unplanned shut-downs and increased maintenance costs.

The corrosivity of the fireside environment in biomass- and waste-fired boilers has been attributed to relatively high levels of alkali chlorides and HCl [1–5]. Indeed, several studies have shown that alkali chlorides accelerate superheater corrosion, with material temperatures in the 400–600 °C range [1, 6–16]. The corrosivity of alkali chlorides toward high-temperature alloys is often explained by a mechanism termed “active oxidation” or the “chlorine cycle” [10–16]. It involves the oxidation of alkali chlorides and/or HCl by O<sub>2</sub> to form molecular chlorine on the scale surface. Cl<sub>2</sub> is then postulated to penetrate the oxide scale and to form volatile transition metal chlorides (e.g., FeCl<sub>2</sub>) at the metal/oxide interface, where the oxygen activity is low [13]. The metal chlorides have high vapor pressures and are suggested to diffuse outward to the scale surface where it decomposes in the more oxygen-rich environment, forming porous oxide. The decomposition releases Cl<sub>2</sub> which may enter the scale again, closing the “chlorine cycle” [14]. This form of the “active oxidation” mechanism has several shortcomings; for example, it does not explain how the highly oxidizing and very reactive Cl<sub>2</sub> molecule can penetrate the scale without being reduced before it reaches the metal. Working with the corrosion of low-alloyed steel in humid air in the presence of KCl, Jonsson et al. [17] and Folkesson et al. [18] proposed a new mechanism that explains alloy chlorination while avoiding some of the contradictions in the traditional “active oxidation” explanation. They proposed that steel chlorination by KCl in an oxygen-rich environment is an electrochemical process which involves cathodic reduction of oxygen at the scale/gas interface and anodic oxidation of iron at the scale/alloy interface. Ionic conduction between the two electrodes was suggested to be provided by transport of Fe<sup>2+</sup> and Cl<sup>−</sup> in the grain boundaries of the oxide scale.

Compared to superheater corrosion, waterwall corrosion in boilers has been much less explored. Low-alloyed steels are often used in waterwalls due to low cost and good mechanical properties. These steels form Fe<sub>2</sub>O<sub>3</sub>/Fe<sub>3</sub>O<sub>4</sub> oxide scales which offer sufficient protection in mildly corrosive environments < 500 °C [19]. Recent studies have shown that KCl does accelerate corrosion of low-alloy steels used for waterwalls in the relevant temperature range (250–400 °C) [17, 18, 20–23]. Thus, exposure of a Fe-2.25Cr-1Mo steel to O<sub>2</sub> and H<sub>2</sub>O at 400 °C in the presence of KCl was reported to result in high corrosion rates accompanied by KCl consumption and chlorination of the alloy [17, 18].

Steel chlorination by HCl(g) has been investigated by several authors [10, 12, 14, 15, 24–30]. Usually, the corrosivity of HCl(g) in air toward steel is attributed to the “chlorine cycle” mechanism cited above. Recently, Folkesson et al. investigated the corrosion of a stainless steel (AISI 310) in a O<sub>2</sub> + N<sub>2</sub> + HCl atmosphere

at 500 °C [29]. They observed a relatively slow alloy chlorination which was suggested to occur by an electrochemical mechanism, similar to that proposed for KCl in [17].

The fireside environment of biomass-fired power plants typically contains a combination of alkali chlorides and HCl(g) in the presence of O<sub>2</sub> and H<sub>2</sub>O. However, to our knowledge the effects of this combination of corrodents on relevant materials have not been studied systematically. Particularly, the role of chlorine-containing compounds in accelerating the corrosion attack needs to be elucidated. The present study is intended to help fill in this apparent knowledge gap by investigating the corrosive effects of the combination of KCl(s) and HCl(g) on a low-alloyed steel at 400 °C.

## Experimental Procedures

The alloy studied is a Fe-2.25Cr-1Mo steel labeled T22; see Table 1 for chemical composition. The geometrical area of the sample was 5.56 cm<sup>2</sup>. A hole ( $\phi = 1.5$  mm) was drilled for ease of handling. Before exposure the samples were ground to 320 grit on SiC and polished with three diamond suspensions 9, 3, and 1  $\mu$ m until the surface appeared mirror-like. The polished samples were degreased and cleaned in acetone and ethanol using ultrasonic agitation. The mass change of the samples was measured prior to and after exposure using a six-decimal Sartorius balance. From the gravimetric results, a theoretical oxide thickness was calculated based on oxide density.

Both a tube furnace and a TGA system (see below) were used for the exposures, and the temperature was kept at  $400 \pm 1$  °C. The reference atmosphere consisted of N<sub>2</sub> with 5% O<sub>2</sub> and 20% H<sub>2</sub>O(g). In the HCl exposures, 500 vppm of HCl(g) was introduced to the reference atmosphere. The flow rate was set to 1000 ml/min, corresponding to 2.5 cm/s. In the KCl exposures, KCl(s) was deposited on the samples *ex situ* by means of spraying a solution of KCl in a 20:80 water–ethanol mixture and subsequently drying with cool air. The amount of salt was applied to result in a weight of 0.1 mg/cm<sup>2</sup> KCl on the surface. Reference samples, without the presence of either KCl(s) and/or HCl(g), were also investigated. The samples exposed in the tube furnace were positioned parallel to the direction of the gas flow, in the center of the furnace. All parts of the system were kept above the dew point of water to prevent condensation. Prior to and after exposure, the samples were stored in desiccators over P<sub>2</sub>O<sub>5</sub>.

**Table 1** Chemical composition of the investigated steel (wt%)

Element	Fe	Cr	Mo	Mn	Si	C	P	S
	96.0	2.2	0.9	0.5	0.3	0.09	0.01	0.01

## Thermogravimetric Analysis (TGA)

A Setaram SETSYS thermobalance was used to study the oxidation kinetics at 400 °C in 5% O<sub>2</sub> + 20% H<sub>2</sub>O and N<sub>2</sub> (in balance) up to 24 h, with and without HCl(g). The water vapor content in the atmosphere was added via a Setaram WET-SYS system. The flow rate was set to 15 ml/min, corresponding to 1.2 cm/s.

## Scanning Electron Microscopy (SEM) and Energy-Dispersive X-ray (EDX)

The samples were characterized using a FEI Quanta ESEM 200, equipped with a field emission gun. The microscope was operated in high vacuum mode. The instrument has an Oxford Inca Energy Dispersive X-ray (EDX) system for chemical analysis. The acceleration voltage was between 8 and 15 kV for imaging and 15 kV for EDX analysis. Backscattered electrons were used for imaging.

## Broad Ion Beam (BIB)

A Leica TIC3X was used for cross section preparation of exposed samples. A 0.5-mm-thick silicon wafer was glued to the sample with Loctite<sup>®</sup> 415. The sample was cut with a low-speed saw without lubrication. The three ion guns were operated at 6.5 kV for a duration of 7 h. The attained cross sections were approximately 500–1000 µm in width.

## X-ray Diffraction (XRD)

A Siemens D5000 powder diffractometer was used to determine crystalline phases present after exposure. The instrument was equipped with a grazing incidence beam attachment together with a Göbel mirror. Cu K<sub>α</sub> radiation ( $\lambda = 1.5418 \text{ \AA}$ ) was used with an angle of incidence 0.5°–2°. The measurement range was  $10^\circ < 2\theta < 65^\circ$ .

## Ion Chromatography (IC)

To determine the amount of Cl<sup>−</sup> after exposure, a Dionex ICS-90 system was used. Cl<sup>−</sup> was analyzed with an IonPac AS4A-SC analytic column, and 1.8 mM Na<sub>2</sub>CO<sub>3</sub> + 1.7 mM NaHCO<sub>3</sub> was used as eluent. The flow rate was 2 mL/min.

# Results

## Gravimetric Analysis

Figure 1 shows the mass gains of a Fe-2.25Cr-1Mo steel exposed for 24 h at 400 °C in four different environments. The lowest mass gain was registered on the sample exposed under reference conditions (i.e., 5% O<sub>2</sub> + 20% H<sub>2</sub>O). Adding 500 vppm HCl(g) to this reference atmosphere resulted in a mass gain which was about twice as high,

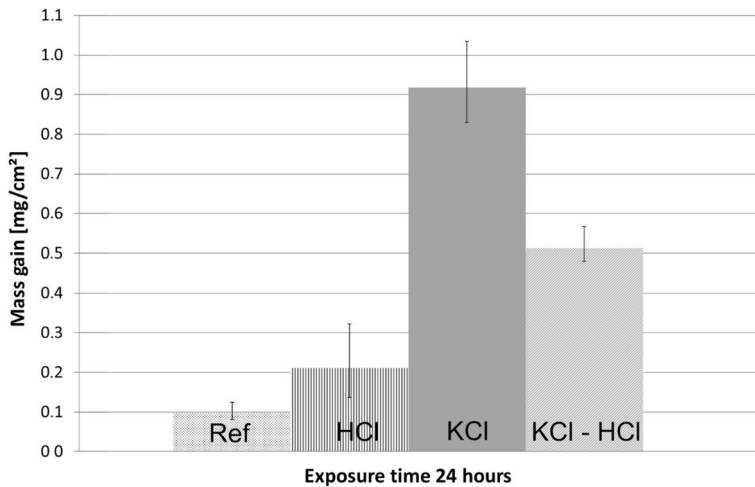


**Fig. 1** Mass gain of a Fe-2.25Cr-1Mo steel exposed for 24 h at 400 °C (tube furnace exposures) exposed in four environments. The values are presented as an average value of at least three samples. The error bars indicate the scatter between the mass gain of individual samples

reaching around 0.2 mg/cm<sup>2</sup> after 24 h. By adding KCl(s) (KCl+5% O<sub>2</sub>+20% H<sub>2</sub>O), the highest mass gain of the investigated environments was recorded. The mass gain is about 0.9 mg/cm<sup>2</sup>. The samples that were exposed to a combination of KCl(s) and HCl(g) exhibited significantly lower mass gain compared to the samples exposed to only KCl(s).

In order to obtain a more detailed information on oxidation kinetics, exposures were carried out in a TG system; see Fig. 2. In general, the mass gains recorded in the TG system are in good agreement with the mass gains acquired in the tube furnace exposures. However, the KCl–HCl exposure shows some deviation between the different exposure systems with respect to final mass gain. As for the tube exposures, the reference and HCl exposures in the TG exhibited the lowest mass gains while the largest mass gains were recorded for the samples exposed in the KCl and KCl–HCl exposures. Even though the KCl- and KCl–HCl-exposed samples are similar (0.98 mg/cm<sup>2</sup> vs. 0.87 mg/cm<sup>2</sup>), the mass gain curves differ greatly. For the sample exposed to KCl only, several “bumps” can be noticed on the mass gain curve and a rather steady overall corrosion rate. The sample exposed in the KCl–HCl exposure, on the other hand, experiences a very rapid mass gain during the first 1–2 h after which the increase in mass is greatly slowed down.

The oxidation kinetics in the TG experiment can be further elucidated by displaying mass gain ( $m$ ) and time ( $t$ ) in a  $\ln(m)$  versus  $\ln(t)$  plot (see Fig. 3). The slope of such plot corresponds to  $1/\alpha$ , where  $\alpha$  is the exponent in the kinetic equation. Thus, a linear mass gain corresponds to  $\alpha=1$  and parabolic mass gain to  $\alpha=2$ :

$$\begin{aligned}
 m^\alpha &\propto t \\
 \alpha \ln(m) &\propto \ln(t) \\
 \ln(m) &\propto 1/\alpha \ln(t)
 \end{aligned}
 \tag{1}$$

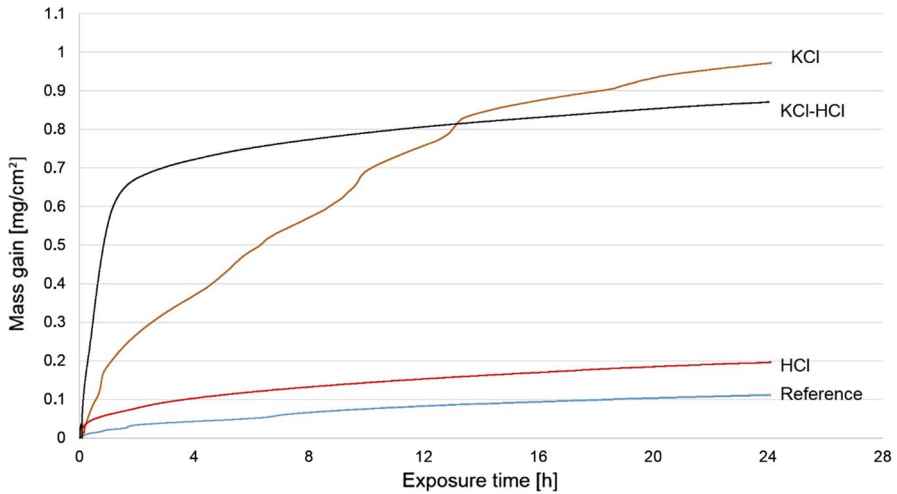


**Fig. 2** Mass gain curves of a Fe-2.25Cr-1Mo steel exposed for 24 h at 400 °C (TG exposures) in four environments

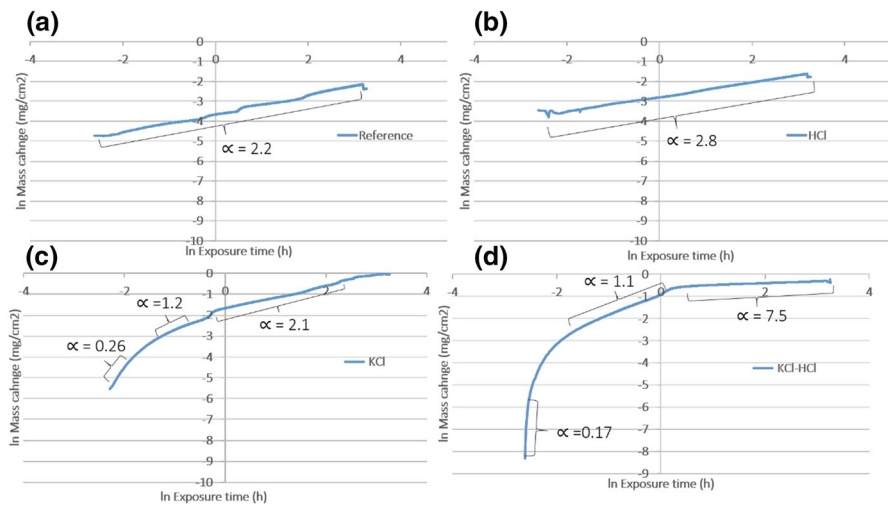


**Fig. 3**  $\ln(m)$  versus  $\ln(t)$  of TG mass gain curves of Fe-2.25Cr-1Mo steel at 400 °C in 5%  $O_2$  + 20%  $H_2O$  + 75%  $N_2$ , **a** reference, **b** with 500 vppm HCl(g), **c** with KCl(s), **d** with KCl(s) – 500 vppm HCl(g). The first 5 min of data in the TG exposures were of relatively poor quality due to the rapid heating and are therefore excluded

Figure 3 shows that both the mass gain of the samples exposed in the reference and the HCl exposures exhibit approximately parabolic or slightly subparabolic behavior throughout the exposures,  $\alpha$  corresponding to 2.2 and 2.8, respectively. In contrast, the plots of the KCl and the KCl–HCl exposures show major changes

of the slope during the experiment, indicating changes in the mechanism of corrosion. Thus, in the KCl plot in Fig. 3c, different stages can be identified. During the early phase, rapid oxide growth is observed with  $\alpha=0.26$ . The slope of the curve then decreases and becomes close to parabolic ( $\alpha=2.1$ ) at  $t>0.7$  h. The KCl–HCl plot initially exhibits very fast kinetics ( $\alpha=0.17$ ). The kinetics then slow down to approximately linear with  $\alpha=1.1$  between  $t=0.2$  h and  $t=1.3$  h. After  $t>1.3$  h the mass gain kinetics become very slow ( $\alpha=7.5$ ).

## Surface Morphology

Figure 4 shows a representative top-view SEM image of the KCl-treated samples prior to exposure. The amount of salt corresponds to  $0.1 \text{ mg/cm}^2$  KCl on the surface, and as seen in Fig. 4, no complete coverage of the sample surface is achieved. Hence, two different areas are recognized: area “1” represents areas covered by KCl crystallites, and area “2” represents areas in between KCl crystallites.

In Fig. 5, the plan view SEM images of the samples exposed for 24 h at  $400^\circ\text{C}$  in the tube furnace can be seen. The image in Fig. 5a depicts the reference sample, showing a rather even and homogenous surface. The surface is covered by an oxide in the form of whiskers. Figure 5b shows the sample exposed in the HCl exposure, exhibiting essentially the same surface morphology as the sample exposed in the reference exposure. Since no KCl was present in these two exposures, only area “2” is noted. The samples exposed in the KCl exposure (see Fig. 5c) showed an irregular and uneven surface where characteristic areas, denoted “1” and “2,” can be discerned. The areas denoted “1” have a rough and undulating morphology and

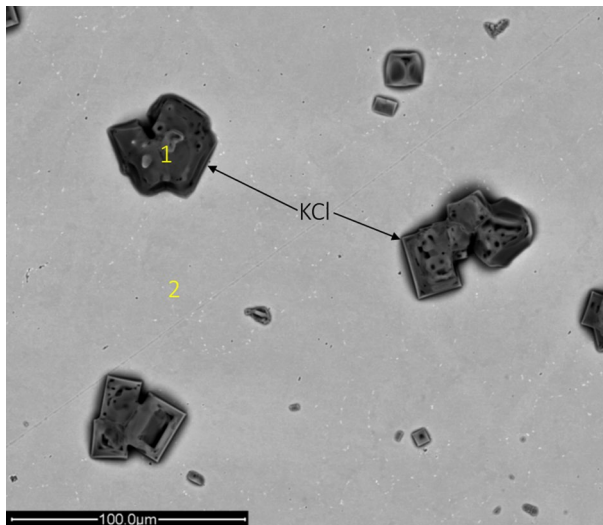


**Fig. 4** Plan view SEM/BSE images of Fe-2.25Cr-1Mo steel with  $0.1 \text{ mg/cm}^2$  KCl added before exposure. The area denoted “1” represents areas covered by KCl crystallites, and the area denoted “2” represents areas in between KCl crystallites



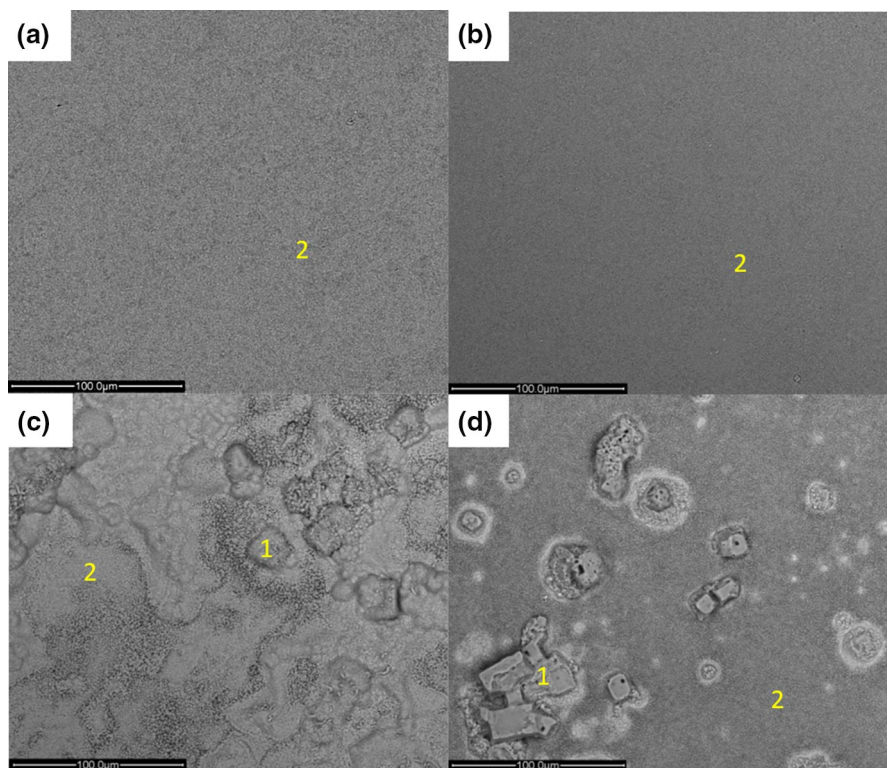


**Fig. 5** Plan view SEM/BSE images of Fe-2.25Cr-1Mo steel after 24 h at 400 °C in 5% O<sub>2</sub>+20% H<sub>2</sub>O + 75% N<sub>2</sub>, **a** reference run, **b** with 500 vppm HCl(g), **c** with KCl, **d** with KCl+500 vppm HCl(g)

correspond to overgrown former KCl particles (compare Fig. 4 with Fig. 5c). The areas denoted “2” in Fig. 5c are located at a distance from the KCl particles and are more even, similar to the reference and HCl exposures.

The sample exposed in the KCl–HCl exposure exhibits a rather different surface appearance compared to the other exposed samples; see Fig. 5d. The KCl crystallites (designated as area “1”) remain to a large degree intact on the surface. This is in contrast to the KCl only exposure where the KCl crystallites are completely overgrown by iron oxide. The area designated “2” in Fig. 5d is similar to the surface observed for this area in the other exposure; the surface morphology is characterized by an even oxide with whiskers.

### Scale Microstructure by BIB Cross Sections

In order to reveal the extent of the corrosion attack of the Fe-2.25Cr-1Mo steel exposed for 24 h at 400 °C in the four investigated environments, BIB cross sections were performed (see Fig. 6). In accordance with the gravimetric and plan view SEM analysis, the samples exposed in the reference exposure (in Fig. 6a) and in the

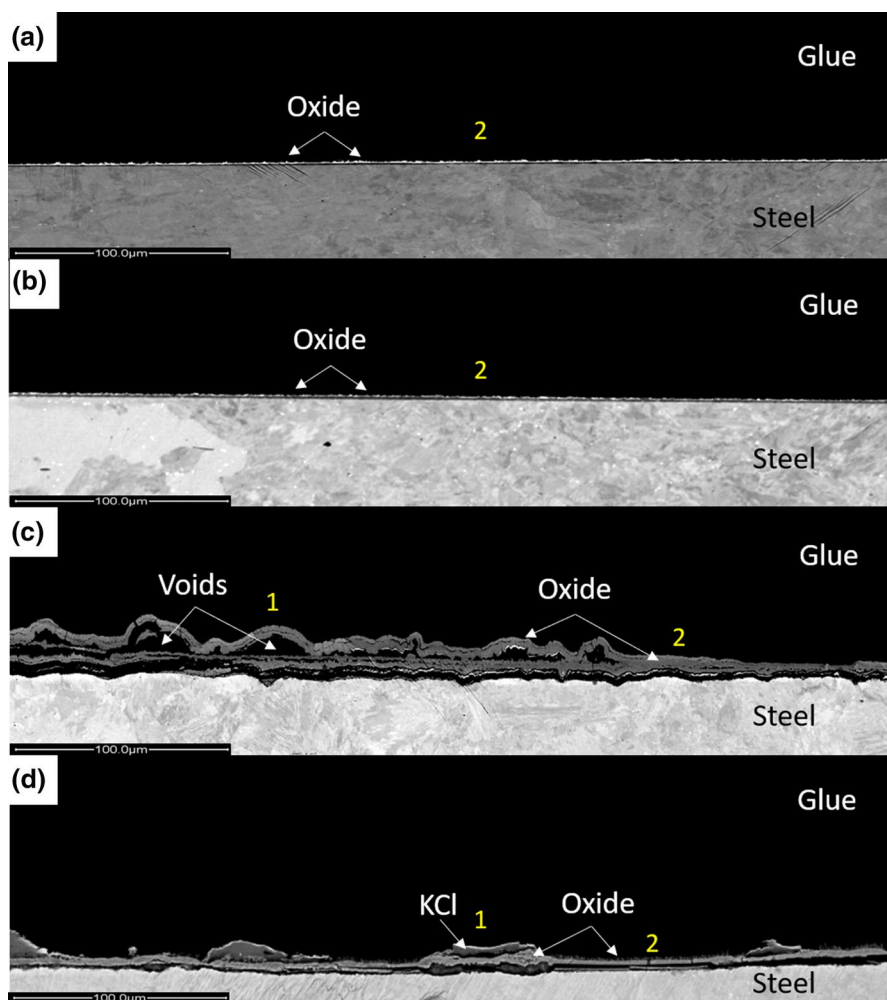


**Fig. 6** BIB cross sections of Fe-2.25Cr-1Mo steel exposed for 24 h at 400 °C in 5% O<sub>2</sub> + 20% H<sub>2</sub>O + 75% N<sub>2</sub> **a** reference run, **b** 500 vppm HCl(g), **c** KCl, **d** KCl + 500 vppm HCl(g)

HCl exposure (Fig. 6b) exhibit thin oxide scales (~1 μm and ~2 μm, respectively). Since no KCl(s) is present, only area “2” exists. In contrast to these samples, the sample exposed in the KCl exposure experienced a much more accelerated corrosion attack.

The BIB cross section of the KCl (only) exposed sample reveals an undulating scale with numerous voids; see Fig. 6c. The area labeled “1” marks the position of a former KCl crystallite, and area “2” corresponds to an area not previously covered by a KCl particle. In area “1”, the corrosion morphology is characterized by a thick scale consisting of several subscales. The outermost scale is undulating and uneven. The inner scales are more even but tend to be delaminated from each other, forming

numerous pores. The area marked “2” in Fig. 6c is denser, and the scales have not delaminated from each other to the same extent. However, pores can also be detected here. In the SEM plan view image (see Fig. 5c), angular oxide agglomerations (area “1”) could be seen which corresponded to former KCl crystallites. According to the cross-sectional view in Fig. 6c, most of these formations were hollow, the KCl particles being fully reacted. However, there were also some KCl particles that only partly reacted and the presence of KCl was evidenced by XRD. The region “2” scale has a typical thickness of 2–3  $\mu\text{m}$ , while the aggregated solid oxide scale in region “1” was 5–10  $\mu\text{m}$ . In area “1” in Fig. 6c, large cracks through the scale can be seen.

In Fig. 6d the cross-sectional view of the sample exposed to KCl–HCl is seen. In contrast to the KCl (only) exposure, the scale has not suffered from delamination and contains few voids. In the SEM plan view image in Fig. 5d, KCl crystallites was seen, seemingly intact, on the surface after exposure. This is verified by the SEM cross section image in Fig. 6d where KCl crystals can be seen on top of the scale (labeled “1”). This is in contrast to the KCl (only) exposure where the KCl crystallites were overgrown by iron oxide. For the KCl–HCl-exposed sample, the scale morphology varies with distance to the KCl particles. Thus, in the vicinity of the KCl particles the scale is relatively thick (5–10  $\mu\text{m}$  in area “1”), while it is thinner (1–3  $\mu\text{m}$ ) and more even at a distance from the KCl particles (area “2”).

## SEM/EDX Analysis of the Scale Microstructure

### Reference and HCl Exposures

In Fig. 7 SEM/EDX images of the cross section of the samples exposed for 24 h at 400 °C in the reference exposure are shown. The scale thickness is 0.5 to 1  $\mu\text{m}$ ,

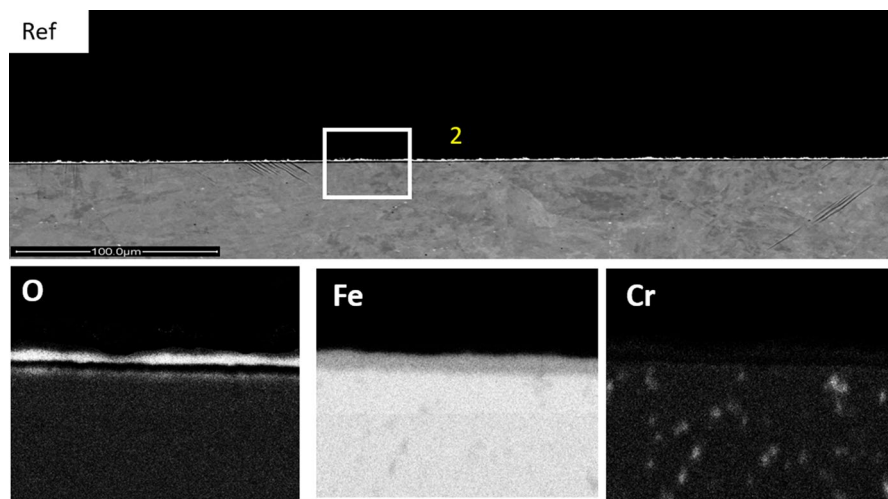


**Fig. 7** BIB cross section SEM/EDX maps of Fe-2.25Cr-1Mo after 24 h at 400 °C in 5% O<sub>2</sub> + 20% H<sub>2</sub>O + 75% N<sub>2</sub> (higher-magnification image of an area in Fig. 7a)

which is in good agreement with the calculated thickness based on the mass gain. According to the XRD analysis, hematite ( $\text{Fe}_2\text{O}_3$ ) and magnetite ( $\text{Fe}_3\text{O}_4$ ) are present. This is in accordance with [18]. Based on the detailed scale analysis in that paper, there is a top layer consisting of hematite while the bottom layer is attributed to magnetite.

The oxide scale formed in the HCl exposure was similar to that observed in the reference exposure; see Fig. 8. However, the thickness was slightly thicker on HCl-exposed sample compared to the corresponding reference-exposed sample, the thickness being 1–2  $\mu\text{m}$  in the HCl exposure. Again, the scale thickness was in good agreement with the measured mass gain. While chlorine was not detected by EDX, small amounts of  $\text{Cl}^-$  were detected by leaching the samples with pure water and analyzing the solution by ion chromatography (IC). The chlorine detected in this way amounted only to 0.3  $\mu\text{mol}$ ; see Fig. 11.

### KCl and KCl + HCl Exposures

Figure 9 shows a SEM/EDX analysis of a BIB cross section of the sample exposed for 24 h at 400 °C in the KCl exposure. The characteristic scale structure

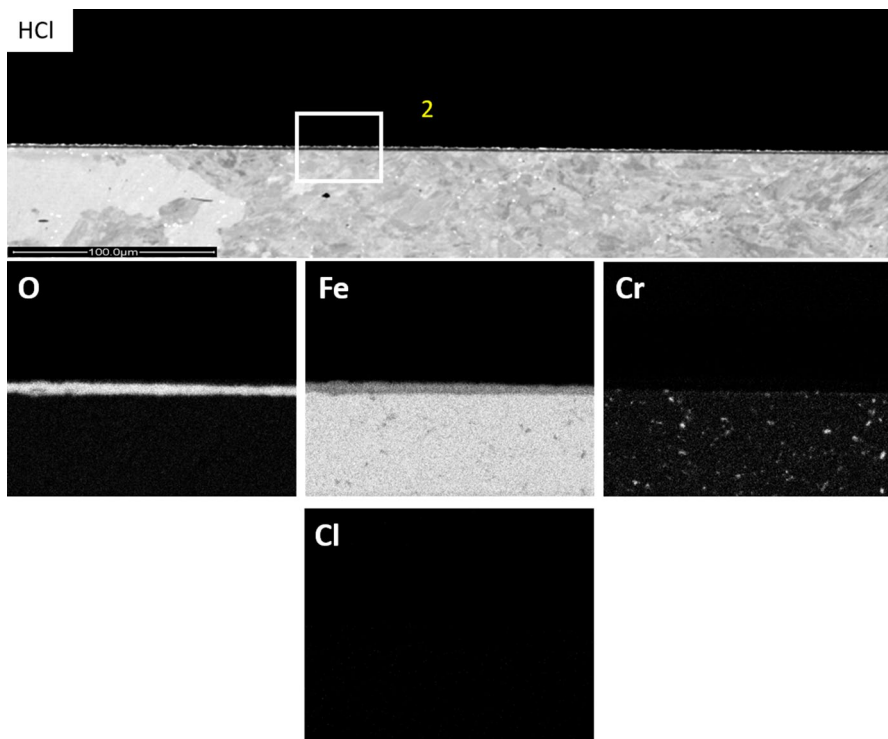


**Fig. 8** BIB cross section SEM/EDX maps of Fe-2.25Cr-1Mo steel after 24 h at 400 °C in 5%  $\text{O}_2$  + 20%  $\text{H}_2\text{O}$  + 75%  $\text{N}_2$  + 500 vppm HCl (higher-magnification image of an area in Fig. 7b)

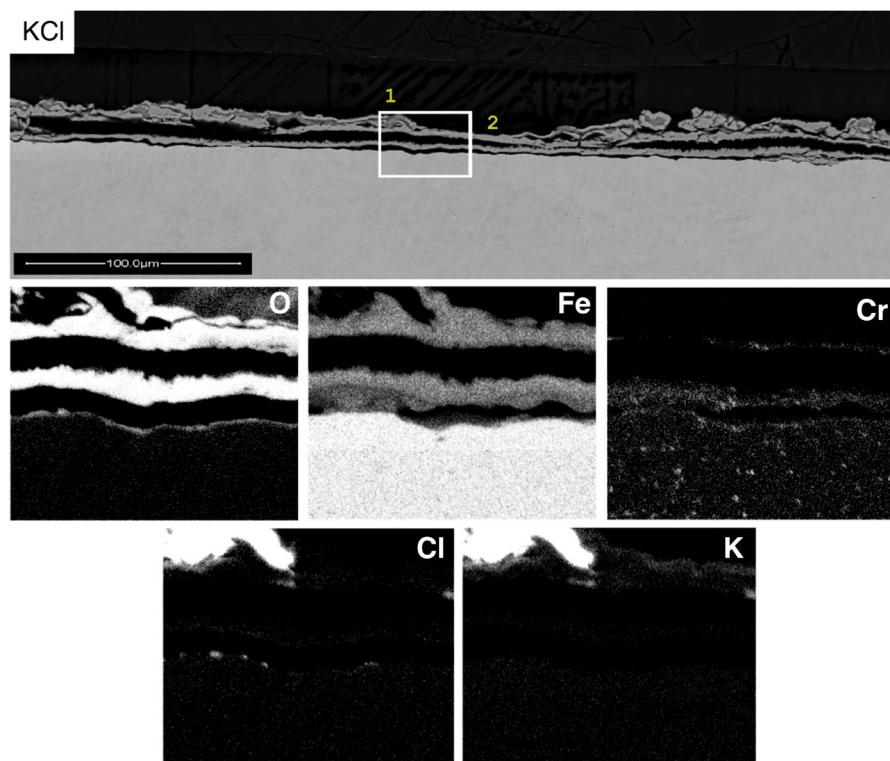


**Fig. 9** BIB cross section and SEM/EDX maps of Fe-2.25Cr-1Mo steel after 24 h at 400 °C in 5% O<sub>2</sub> + 20% H<sub>2</sub>O + 75% N<sub>2</sub> + KCl (higher-magnification image of an area in Fig. 7c)

seen in Fig. 6c consisting of consecutive, partly delaminated subscales is reflected in the Fe and O maps. There is an overlap between the potassium and chlorine maps, implying the presence of a KCl particle. However, other regions where the KCl particles have reacted completely do also exist. The top part(s) of the oxide scale, i.e., away from the KCl particle, is containing trace amounts of potassium (whereas no signal from chlorine was detected). Based on the resolution of the EDX analysis, the presence of potassium is hard to quantify. In a recent paper, however, TEM analysis of this sample quantified the amount of potassium to 1% (atomic) and the absence of chlorine in these layers was confirmed [31]. In the Cr map in Fig. 9 a, thin straight band can be seen in the lower part of the outermost oxide layer. This band is suggested to correspond to the former metal surface, marking the interface between outward-growing and inward-growing oxide. Potassium was not detected below this Cr rich band. Local chlorine accumulations were detected at the scale/alloy interface. The absence of other elements than Fe at these sites allows us to interpret these enrichments as iron chloride (FeCl<sub>2</sub>). The amount of chlorine still present on the sample is, according to the IC analysis in Fig. 11, about 2.5 μmol. This corresponds to about 36% of the amount

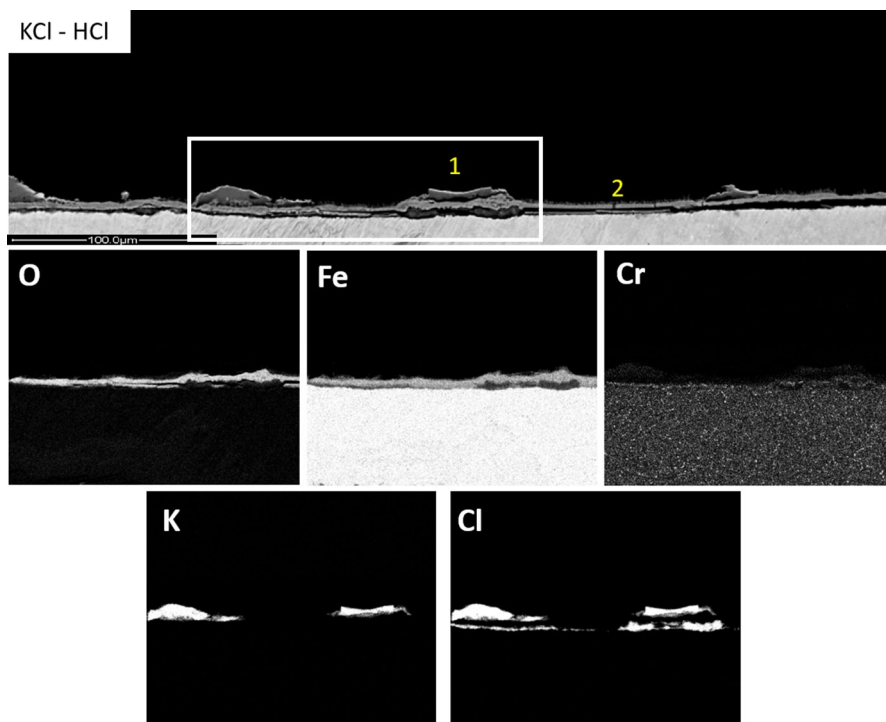


**Fig. 10** BIB cross section SEM/EDX maps of Fe-2.25Cr-1Mo steel after 24 h at 400 °C in 5% O<sub>2</sub>+20% H<sub>2</sub>O+75% N<sub>2</sub>+KCl+HCl(g) (higher-magnification image of an area in Fig. 7d)

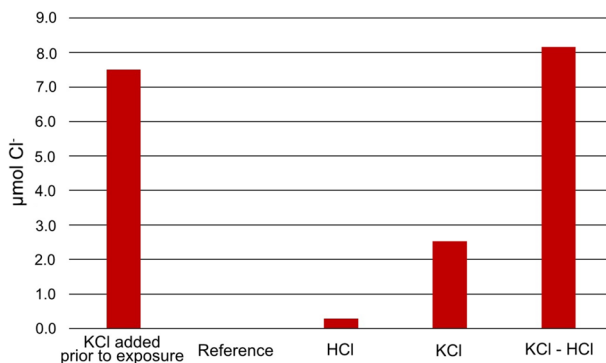


**Fig. 11** Amount of chloride on the samples before and after exposure. The “unexposed” value corresponds to the KCl added in the KCl and in the KCl–HCl(g) exposures. The measurements after the exposure were performed by ion chromatography analysis for water-soluble ions

of KCl(s) added prior to exposure. (7.0 μmol KCl(s) was sprayed on the sample prior to exposure.)

In Fig. 10 the SEM/EDX images of the BIB cross section of the sample exposed in the KCl–HCl exposure are seen. Compared to the corresponding sample exposed



in the KCl (only) exposure, the scale is thinner and denser. In particular, the delamination of oxide scales seen in the KCl (only) exposure is not equally pronounced in the KCl–HCl exposure. The K and Cl EDX maps in Fig. 10 are overlapping, indicating the presence of unreacted KCl particles remaining on the top surface. In addition, beneath the KCl crystallites the Cl map shows relatively large chlorine enrichments, not associated with potassium. These chlorine enrichments form more or less continuous layers at the bottom of the scale in the vicinity of the KCl crystallites. The Cl concentration in this layer reaches approximately 35 at %. Moving away from the KCl crystallites, the amount of chlorine at the bottom of the scale decreases rapidly. The high concentration of chlorine and the lack of potassium in this region allow us to conclude that this subscale layer consists of  $\text{FeCl}_2$ . The IC analysis in Fig. 11 shows that the amount of Cl is much higher on the samples exposed in the KCl–HCl exposure compared to the samples exposed in the KCl exposure. Indeed, the amount of chlorine detected in the leach water from the samples exposed in the KCl–HCl exposure was somewhat greater than the amount added before exposure in the form of KCl. In contrast to the sample exposed in the KCl exposure, there was no evidence for potassium in the top iron oxide layer on the sample exposed in the KCl–HCl exposure. All potassium detected by EDX was overlapping with the chlorine map, indicating the presence of KCl(s).

According to the mass gain curves presented in Fig. 2, the samples exposed in the KCl and the KCl–HCl exposure exhibit similar mass gains after 24 h. However, the kinetics of the corrosion attack in two exposures differs substantially. After about 1 h, the mass gain of the sample exposed in the KCl–HCl exposure is almost 3 times as high. In order to investigate the initiation of the corrosion attack, additional samples exposed only for 1 h in the KCl and the KCl–HCl exposures, respectively, were performed. The SEM/EDX analysis (both plan view and cross sections) of the sample exposed in the KCl exposure is shown in Fig. 12. The corresponding sample exposed in the KCl–HCl exposure is seen in Fig. 13.

The sample exposed in the KCl (only) exposure shows already after 1-h exposure at 400 °C that the sample surface has started to corrode (see the plan view SEM image in Fig. 12). The surface in between the KCl crystallites is somewhat undulating, and corrosion products have started to form. Some of the KCl crystallites remain relatively unreacted, whereas some KCl particles have become overgrown. In the BIB cross section (Fig. 12), the extent of the corrosion attack is more visible. The cross section reveals a rather undulating surface where some areas are covered by a thick, delaminated oxide layer. The oxide layer in other areas is still rather thin and well adherent. The EDX analysis reveals unreacted KCl, incorporated by iron oxide. There are no signs of metal chlorides.

The sample exposed in the KCl–HCl exposure shows a slightly different corrosion attack compared to the corresponding sample exposed in the KCl (only) exposure (compare Fig. 12 and Fig. 13). After 1-h exposure at 400 °C KCl–HCl exposure (see top SEM plan view image in Fig. 13), the corrosion attack of the sample is rather uneven. In the close vicinity to the KCl particles, corrosion products have formed whereas the area in between KCl crystallites seems rather unaffected. The difference in the corrosion attack between different areas of the sample is more clearly seen in the BIB cross section (see Fig. 13). In association with the KCl crystallites, a

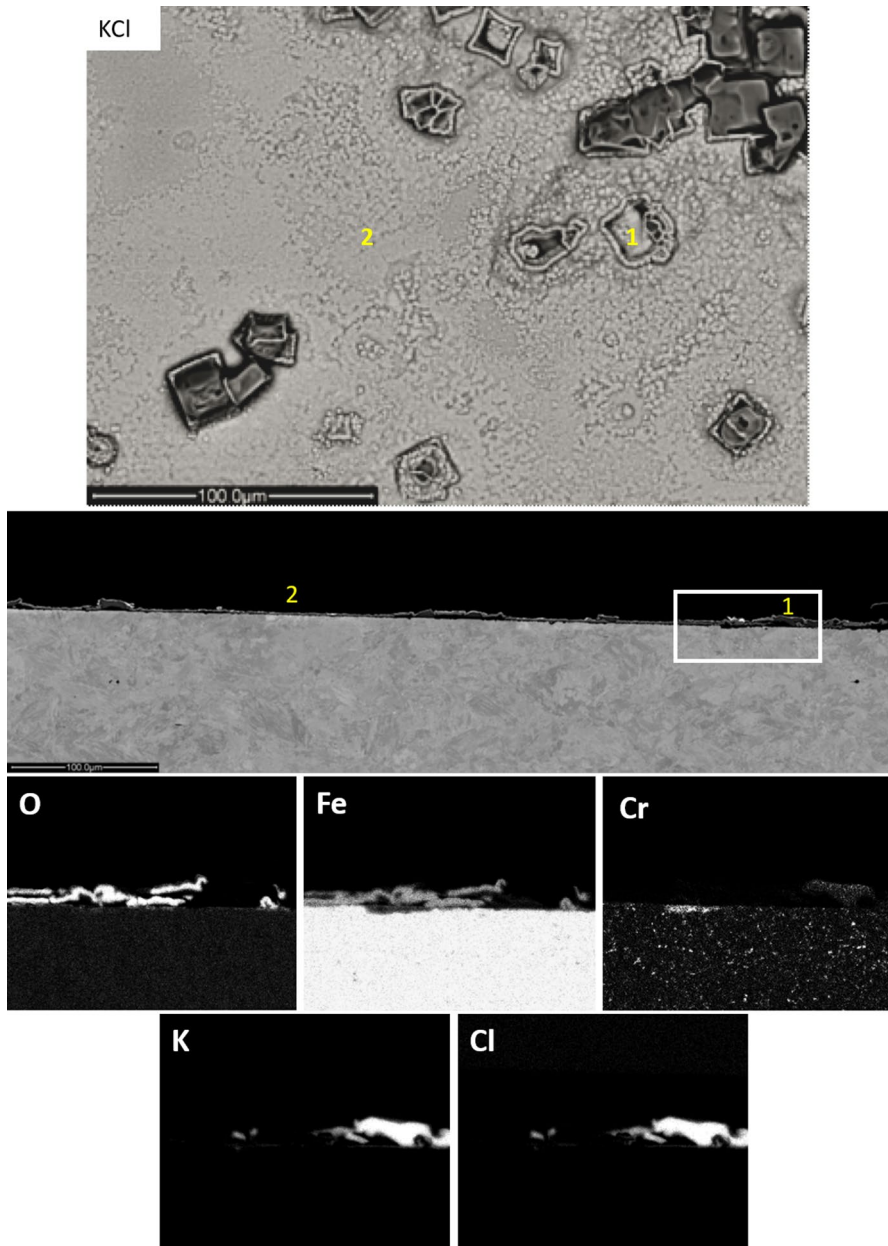


**Fig. 12** Plan view SEM/BSE and cross-sectional SEM/EDX analysis of Fe-2.25Cr-1Mo steel after 1 h at 400 °C in 5% O<sub>2</sub> + 20% H<sub>2</sub>O + 75% N<sub>2</sub> + KCl

thick corrosion product layer has formed. According to the EDX analysis, the inner part of this layer is iron chloride. On top, an iron oxide layer is detected. The SEM/EDX analysis performed, both as cross sectional and as plan view, indicated that the



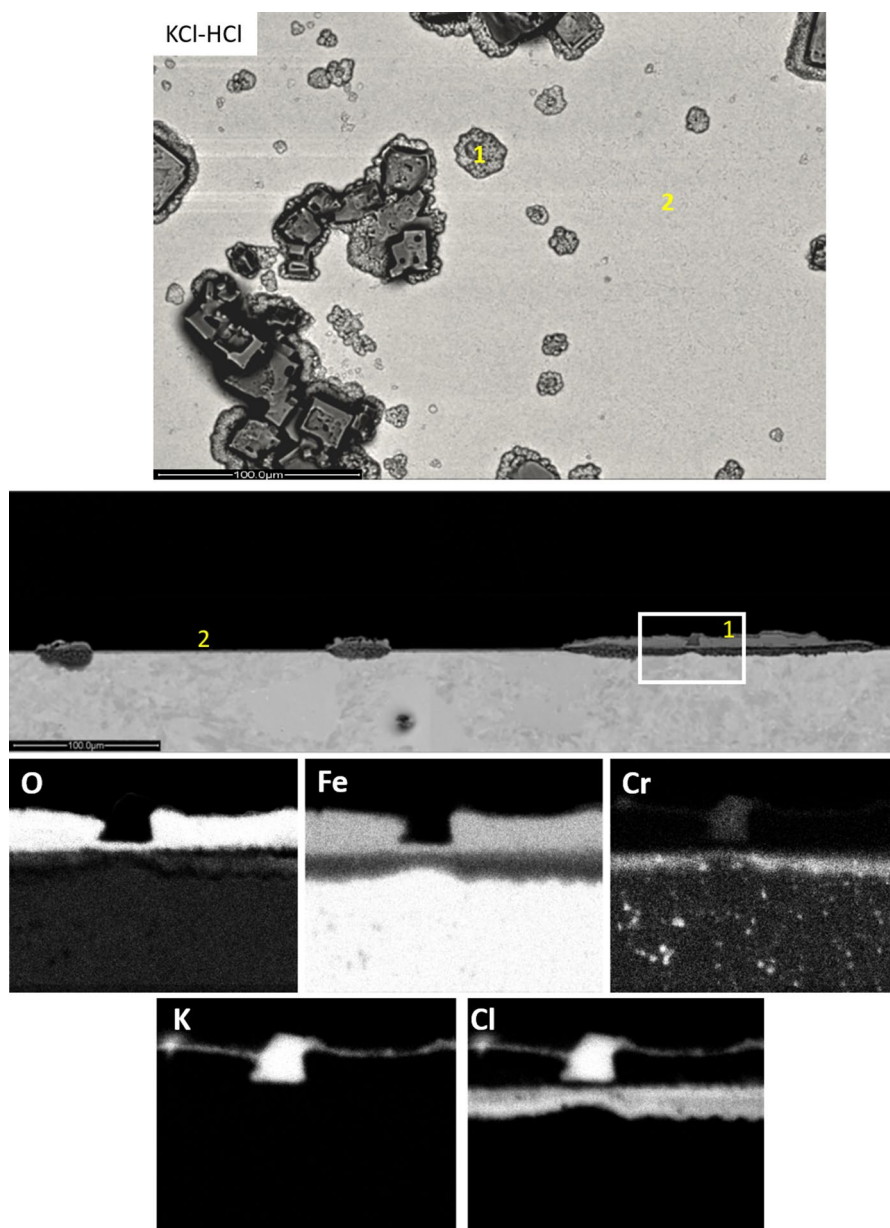


**Fig. 13** Plan view SEM/BSE and cross-sectional SEM/EDX analysis of Fe-2.25Cr-1Mo steel after 1 h at 400 °C in 5% O<sub>2</sub> + 20% H<sub>2</sub>O + 75% N<sub>2</sub> + KCl + HCl(g)

KCl crystallites were more intact compared to the corresponding sample in the KCl exposure. A close-up of the corrosion attack in the vicinity of the KCl crystallite on the sample exposed in the KCl–HCl exposure is seen in Fig. 14.

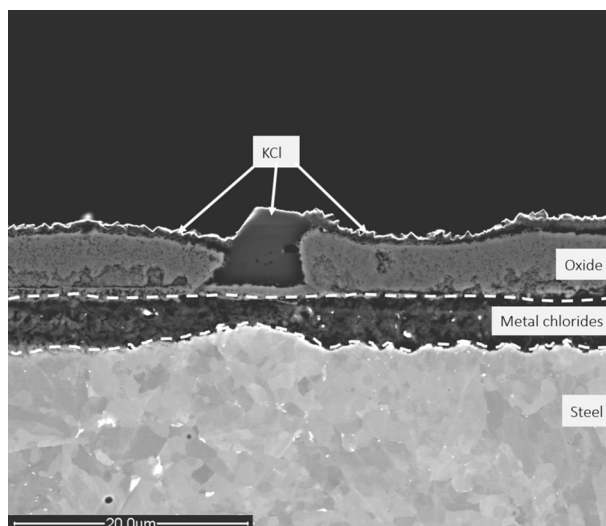


**Fig. 14** Cross-sectional SEM image of Fe-2.25Cr-1Mo steel after 1 h at 400 °C in 5% O<sub>2</sub>+20% H<sub>2</sub>O+75% N<sub>2</sub>+KCl+HCl(g)

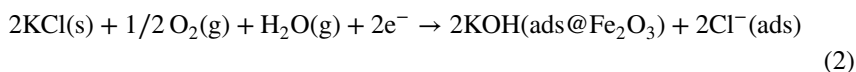
## Discussion

In accordance with previous reports on the oxidation properties of low-alloyed steel [18] and as expected considering the widespread use of the material (a Fe-2.25Cr-1Mo steel) in this temperature range, the reference exposure (24 h in 5% O<sub>2</sub>+20% H<sub>2</sub>O+75% N<sub>2</sub> at 400 °C) resulted in the formation of a protective and adherent oxide scale with a thickness in the range 0.5–1 μm. The scale microstructure was investigated in detail in a previous paper [18]. The scale was reported to consist of an inward-growing, chromium-containing magnetite ((Fe,Cr)<sub>3</sub>O<sub>4</sub>) layer and an outward-growing part made up of a (middle) Fe<sub>3</sub>O<sub>4</sub> and a (top) Fe<sub>2</sub>O<sub>3</sub> layer.

As expected, KCl strongly accelerated corrosion and had a major effect on scale morphology, resulting in the formation of a porous and delaminated scale; see Fig. 9. Alloy chlorination was evidenced by the observation of small amounts of FeCl<sub>2</sub> at scattered locations at the steel/scale interface, while an excess of potassium (not accompanied by chlorine) was detected at the top surface. Jonsson et al. [17] and Folkesson et al. [18] reported that the corrosion of steel in KCl+O<sub>2</sub>+H<sub>2</sub>O environment starts at about 350 °C, being accompanied by consumption of KCl and formation of iron oxide on the KCl crystallites. The behavior was attributed to the formation of a thin liquid KCl/FeCl<sub>2</sub> film on the scale surface. (The eutectic temperature is 355 °C.) The accumulation of iron oxide at the KCl particles was explained by rapid diffusion of FeCl<sub>2</sub> in the liquid film toward the KCl crystallites where it decomposes to hematite+HCl(g) (see below). The present study corroborates the findings in [17, 18], e.g., see Fig. 5 showing the formation of iron oxide precipitates on the former KCl crystallites.

In accordance with [17, 18], the SEM/EDX analysis of the sample from the KCl exposure (Fig. 9) indicates that potassium is enriched in the top part of the delaminated oxide scale. This is in accordance with a TEM/EDX analysis of the sample [31], showing that the top of the iron oxide layer was enriched in potassium but not in chlorine, implying that alkaline conditions persist at the scale/gas interface. The accumulation of potassium at the scale surface is predicted by the electrochemical mechanism for alloy chlorination [17, 18]. Adapting the corrosion mechanism presented in [17, 18] to the observations in the present paper, the following electrochemical corrosion reaction is proposed:

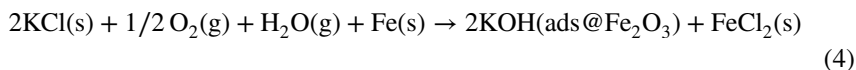
Cathodic reaction (at the scale surface):



Anodic reaction (at the scale/alloy interface):



Cell reaction:



The proposed reaction scheme was investigated in a recent paper, using first principles calculations [32]. The paper considers a case where chloride ions are transported by solid state transport across a scale consisting of a magnetite monocystal. It concludes that alloy chlorination by the above scheme is thermodynamically viable.

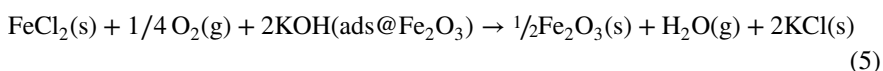
It may be noted that the proposed electrochemical reaction includes formation of  $\text{KOH(ads@Fe}_2\text{O}_3)$  which denotes potassium hydroxide chemisorbed on hematite. To justify why this species was selected to represent excess potassium on the scale surface, it is first pointed out that formation of pure KOH can be ruled out because thermodynamical calculations show that under the experimental conditions, iron chlorination by KCl (corresponding to reaction 4) is not spontaneous if  $\text{KOH(s)}$  is formed. Hence, in order for iron chlorination to be spontaneous, the excess potassium on the surface must form a compound which is considerably more stable than pure  $\text{KOH(s)}$ .

One possibility is that the excess potassium forms one of the several potassium iron (III) oxides described in the literature [33–36]. Among them, potassium ferrite(III),  $\text{KFeO}_2$  and  $\beta$ -potassium ferrite,  $\text{K}_2\text{Fe}_{22}\text{O}_{34}$ , are well known as active components in many catalysts, e.g., in the ammonia synthesis and in various petrochemical processes [37, 38]. However, it has been reported that temperatures of about 600 °C are needed to synthesize crystalline  $\text{KFeO}_2$  while even higher temperatures are needed for forming  $\beta$ -potassium ferrite [39]. Also, Muhler et al. [37] report that at 320 °C,  $\text{KOH(s)}$  does not react with hematite to form ferrite but is instead chemisorbed on hematite. Investigating the properties of  $\text{KFeO}_2$  and  $\beta$ -potassium ferrite and comparing them to KOH-doped hematite, Kotarba et al. [40] reported that small amounts of adsorbed KOH (1–2  $\text{K}^+$  per  $\text{nm}^2$ ) on hematite do not react to form bulk potassium ferrite, even at high temperatures. Indeed, [30] shows that  $\text{K}^+$  adsorbed on hematite is more strongly

bonded than potassium ions in the bulk ferrites. The strong bonds formed between  $K^+$  and hematite and the reported lack of further reaction of adsorbed KOH with hematite indicate that  $KOH(ads@Fe_2O_3)$  is thermodynamically favored over, e.g.,  $KFeO_2$ .

Considering that the potassium concentrations detected in the top (hematite) part of the scale (1 at % according to [31]) are too low to be compatible with any known potassium ferrite and that there was no indication for potassium ferrite by XRD, it is proposed that the excess potassium in the outer part of the iron oxide scale is chemisorbed on hematite. The formula  $KOH(ads@Fe_2O_3)$  highlights that KOH is not physically adsorbed on the surface but is strongly bonded (=chemisorbed) on hematite. Because the thermodynamic properties of  $KOH(ads@Fe_2O_3)$  have not been reported, the thermodynamic driving force for reactions involving this species cannot be calculated.

In the electrochemical corrosion cell (see reaction 2–4),  $FeCl_2$  forms by combining  $Fe^{2+}$  and  $Cl^-$  ions, the locus of  $FeCl_2$  formation depending on the relative rates of inward chlorine transport and outward transport of ferrous ion. Accordingly,  $FeCl_2$  may form both at the scale surface and at the scale/alloy interface; see discussion in [15]. The lack of evidence for  $FeCl_2$  on the top surface may be due to hydrolysis (see above), volatilization and/or reaction with the excess potassium. Pure KOH reacts spontaneously with iron chloride, forming iron (II) hydroxide and KCl [41]: The reaction is essentially a neutralization reaction, being strongly exothermic ( $\Delta G_{400\text{ }^\circ\text{C}}^\circ = -231.8\text{ kJ/mol}$ , [42]). Considering that iron hydroxides spontaneously decompose into iron oxide and water vapor at the temperature of interest, it is proposed that  $KOH(ads@Fe_2O_3)$ , postulated to form in the present case, reacts in a similar way:

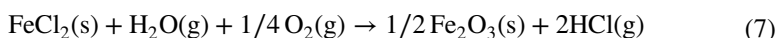


It may be noted that reaction (5) does not result in the loss of chlorine from the surface. However, only 1/3 of the chlorine added as  $KCl(s)$  prior to the exposure was detected by IC analysis after exposure (see Fig. 11). Analysis by XRD and SEM/EDX showed that the chlorine detected after exposure was present both as KCl and  $FeCl_2$ . The vapor pressure of KCl at 400 °C is negligible ( $< 10^{-9}$  bar). Thermodynamic calculations show that direct volatilization of  $FeCl_2$  is also rather low:



$$p_{eq}(FeCl_2) = 0.41 \cdot 10^{-6} \text{ bar at } 400\text{ }^\circ\text{C}$$

In contrast, the hydrolysis of  $FeCl_2$  (as proposed by [15]) is thermodynamically strongly favored in the investigated environment:



$$\Delta G_{400\text{ }^\circ\text{C}}^\circ = -209\text{ kJ/mol.}$$

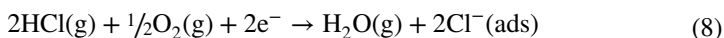
On the basis of this discussion, it is concluded that  $FeCl_2$  is hydrolyzed on the surface, explaining both the net loss of chlorine from the samples and the observation of iron oxide rims on partly reacted (and former) KCl particles.

Thus, it is proposed that alloy chlorination in the KCl (only) exposure occurs by reactions (2)–(4) and that  $\text{FeCl}_2$  is only detected at the scale/alloy interface because  $\text{FeCl}_2$  which is formed at the surface either reacts with the excess potassium according to reaction (5) or is hydrolyzed according to reaction (7).

As noted in the Results section, the TG curve in the KCl (only) exposure, together with the presence of a sequence of multiple oxide layers in the resulting scale, implies recurrent breakdowns of the oxide scale. It is suggested that the breakdown events correspond to scale cracking which leads to a sudden acceleration of oxidation due to the penetration of  $\text{O}_2$  and  $\text{H}_2\text{O}$  through the cracks. The volume expansion associated with  $\text{FeCl}_2$  formation ( $V(\text{FeCl}_2)/V(\text{Fe})=5.6$ ) may be a possible reason for scale cracking. However, this is considered unlikely because scale cracking was only observed in the KCl (only) exposure where small amounts of subscale chloride were detected and not in the KCl + HCl exposure where large amounts of  $\text{FeCl}_2$  were observed below the scale. Instead, it is suggested that scale cracking is promoted by the alkaline conditions (the presence of adsorbed KOH) in the top part of the oxide scale. Thus, it is hypothesized that crack formation in the oxide scale is energetically favored by the presence of adsorbed KOH which tends to react with the free oxide surface created when a new crack forms.

The present results show that 500 vppm HCl has much less effect on the initial oxidation behavior of a Fe-2.25Cr-1Mo steel exposed at 400 °C than KCl(s). Thus, the scale microstructure after the HCl exposure was similar to that observed after the reference exposure, except that the oxide scale was about twice as thick, in the range 1–2  $\mu\text{m}$ . There is relatively little information on the effect of HCl(g) on the corrosion behavior of iron and low-alloyed steels in the presence of  $\text{O}_2$ . Pastén et al. [30] investigated the corrosive effect of HCl(g) toward a wide range of alloys. In accordance with the present study, they report that exposure of carbon steel to HCl-containing environments did not result in chloride-containing scales and that the corrosion accelerating effect of HCl was small in comparison with the corrosive effect of some alkali salts. However, the additional presence of  $\text{SO}_2$  and salts in the experiments in [30] makes it difficult to compare their work with the present study. While chlorine was not detected in the cross section analysis of the sample exposed (see Fig. 8), small amounts were detected by IC analysis for water leachable ions (see Fig. 11). It is suggested that small amounts of chlorine do enter the scale and that the lack of evidence for it by SEM/EDX implies that the amount of iron chloride is below the limit of detection. Investigating the chlorination of a stainless steel (AISI 310) in 500 vppm HCl in  $\text{O}_2 + \text{N}_2$  environment at 500 °C, Folkesson et al. detected transition metal chlorides both on top of the thin oxide scale and below this scale [29]. They proposed that alloy chlorination occurred by the following electrochemical corrosion cell:

Cathode (scale/gas interface):



Anode (scale/alloy interface, Fe used as an example):



Cell reaction:



Similar to [17], the authors postulated that anode and cathode are connected by transport of chloride and ferrous ions via the grain boundaries in the oxide scale and electronic conduction through the oxide. As mentioned above, the recent first principles study of the chlorination of iron by KCl in the presence of  $\text{O}_2$  [32] indicates that chloride ions can penetrate a magnetite scale by bulk diffusion, implying that chloride ion transport need not be confined to the grain boundaries in the oxide scale. A comparison of steel chlorination by  $\text{HCl(g)}$  with chlorination by  $\text{KCl(s)}$  (see reactions 2–4) shows that the former occurs in an acidic environment [in the presence of  $\text{HCl(g)}$ ] while the latter generates alkaline conditions ( $\text{KOH}$ ) on the scale surface. The relatively low corrosivity of  $\text{HCl(g)}$  in comparison with  $\text{KCl(s)}$  in this study is tentatively attributed to the fact that while the activity of KCl on the scale surface reaches unity, the activity of  $\text{HCl(g)}$  is only  $5 \times 10^{-4}$ . It is suggested that  $\text{O}_2$  and especially  $\text{H}_2\text{O}$  prevail over  $\text{HCl}$  in the competition for adsorption sites on the scale surface. This would impede chlorination because  $\text{HCl(g)}$  must be bonded to the surface to take part in the cathodic process (see reaction 8). The lack of evidence for  $\text{FeCl}_2$  in this study, as opposed to the detection of transition metal chlorides in [24], is attributed to the lower temperature which causes chlorination to be slower.

The effect of combining the two chlorinating agents  $\text{KCl(s)}$  and  $\text{HCl(g)}$  is striking, scale morphology being very different from both the KCl (only) and the  $\text{HCl}$  (only) exposures. Notably, the scale morphology is reminiscent of scales reported for samples exposed in waste-fired boilers [21]. Considering the mass gain after 24 h and the evidence for alloy chlorination, the combination of corrodents is somewhat similar to the KCl exposure. However, the amount of  $\text{FeCl}_2$  detected on the sample in the KCl–HCl exposure is much greater compared to the KCl (only) exposure (compare Fig. 9 and 10). Thus, a thick  $\text{FeCl}_2$  subscale was detected in the vicinity of the KCl particles in the former case, while only small amounts of  $\text{FeCl}_2$  were detected after the KCl (only) exposure. Importantly, the oxide scale formed in the KCl–HCl exposure appears to be free of cracks, while the KCl (only) exposure resulted in a porous and cracked scale. Also, the KCl crystallites are only little affected in the KCl–HCl exposure. The mass gain curves in Fig. 2 and the plots in Fig. 3 reveal that the kinetics of oxidation are also very different in the two cases. Thus, while mass gain is initially much faster in the KCl–HCl exposure, the mass gain curve levels off after about one hour so that the largest mass gain after 24 h is registered in the KCl (only) exposure.

In comparison with the KCl exposure described above, the corrosion chemistry of the KCl–HCl exposure mainly differs with respect to the situation in the top part of the scale. Thus,  $\text{HCl(g)}$  will tend to react with and neutralize any excess potassium in the top part of the scale:



The consumption of the excess potassium according to reaction (11) will depolarize the cathodic reaction (2), thereby speeding up the electrochemical corrosion process. This effect is suggested to explain why mass gain in the KCl–HCl exposure is initially much faster than in the KCl (only) exposure.

Hence, the accumulation of much larger amounts of  $\text{FeCl}_2$  at the bottom of the scale in the  $\text{KCl-HCl}$  exposure compared to the  $\text{KCl}$  (only) exposure is attributed to the presence of  $\text{HCl}$ , which speeds up reactions (2)–(4) by reacting with the excess potassium at the scale/gas interface. As mentioned above, the repeated cracking of the scale in the  $\text{KCl}$  (only) exposure is suggested to be due to the excess potassium in the top part of the scale. Hence, the absence of scale cracking in the  $\text{KCl-HCl}$  exposure is attributed to the neutralization reaction (11). The thick subscale  $\text{FeCl}_2$  layer in the  $\text{KCl-HCl}$  exposure is also considered significant. Thus, it may be noted that Wagner-type scale growth ceases if the ionic *or* the electronic conduction paths (connecting the gas/oxide and the metal/oxide interfaces) are interrupted. Because  $\text{FeCl}_2$  is reportedly an electronic insulator, while being a good ionic conductor [19], it is suggested that the rapid deceleration of the mass gain in the  $\text{KCl-HCl}$  exposure is due to the formation of an electronically insulating  $\text{FeCl}_2$  layer at the bottom of the scale. In this way, the electrochemical corrosion cell between the  $\text{O}_2$  at the scale surface and the iron electrode at the bottom of the scale, which is responsible for  $\text{FeCl}_2$  formation in the first place, becomes disconnected. Thus, the electrochemical process in the  $\text{KCl-HCl}$  exposure is suggested to be essentially the same as in the  $\text{KCl}$  (only) exposure, i.e., reactions (2)–(4) with the exception of the neutralizing effect of  $\text{HCl(g)}$  in reaction (11). The much faster initial chlorination in the  $\text{KCl-HCl}$  exposure is attributed to a faster cathodic reaction caused by the same neutralization process which causes the cathodic process to be depolarized.

## Conclusions

- Exposing a Fe-2.25Cr-1Mo steel to a combination of  $\text{KCl(s)}$ ,  $\text{O}_2(\text{g})$  and  $\text{H}_2\text{O(g)}$  at 400 °C results in an electrochemical corrosion process involving the formation of chemisorbed  $\text{KOH}$  on the scale surface and solid  $\text{FeCl}_2$ .
- The process is accompanied by extensive cracking and delamination of the iron oxide scale, resulting in a very complex and convoluted scale morphology.
- The addition of 500 vppm of  $\text{HCl(g)}$  to the above resulted in major changes in the corrosion process:
  - Initially, the electrochemical corrosion process is accelerated because  $\text{HCl}$  reacts with the  $\text{KOH}$  released at the scale surface, causing the cathodic process to be depolarized. Thick  $\text{FeCl}_2$  layers form at the scale/alloy interface, beneath the  $\text{KCl}$  crystallites.
  - After the initial step, the corrosion rate is greatly reduced. This is attributed to the electronically insulating nature of the  $\text{FeCl}_2$  layer which causes the cathode at the scale surface in the vicinity of the  $\text{KCl}$  particles to become disconnected from the anode directly beneath.
- In the absence of  $\text{KCl}$ , the addition of 500 vppm  $\text{HCl(g)}$  to the  $\text{O}_2 + \text{H}_2\text{O}$  environment has only minor effects on mass gain and scale morphology.
- The high corrosivity of  $\text{KCl(s)}$  in comparison with  $\text{HCl(g)}$  is attributed to the formation of  $\text{KOH}$  in the former case and to the higher activity of  $\text{KCl(s)}$  in comparison with  $\text{HCl(g)}$ .



**Acknowledgements** Open access funding provided by Chalmers University of Technology. This work was carried out at the Swedish High Temperature Corrosion Centre (HTC) at Chalmers University of Technology and is hereby gratefully acknowledged together with Swedish Energy Agency and the member companies (AB Sandvik Materials Technology, Kanthal AB, Energiforsk AB, MH Engineering AB, Thermo-Cale Software AB, Valmet Technologies Oy, Sumitomo SHI FW Energia Oy, Babcock and Wilcox Volund AS and Maabjerg Energy Center Holding A/S). This work was performed in part at the Chalmers Materials Analysis Laboratory, CMAL.

**Open Access** This article is distributed under the terms of the Creative Commons Attribution 4.0 International License (<http://creativecommons.org/licenses/by/4.0/>), which permits unrestricted use, distribution, and reproduction in any medium, provided you give appropriate credit to the original author(s) and the source, provide a link to the Creative Commons license, and indicate if changes were made.

## References

1. J. Pettersson, C. Pettersson, N. Folkesson, L. G. Johansson, E. Skog and J. E. Svensson, *Materials Science Forum* **522–523**, 563 (2006).
2. F. J. Frandsen, *Fuel* **84**, 1277 (2005).
3. M. Spiegel, C. Schroer and H. J. Grabke, *Materials Science Forum* **251–254**, 527 (1997).
4. P. Viklund, A. Hjornhede, P. Henderson, A. Stalenheim and R. Pettersson, *Fuel Processing Technology* **105**, 106 (2013).
5. S. Karlsson, L. E. Amand and J. Liske, *Fuel* **139**, 482 (2015).
6. J. Lehmusto, B. J. Skrifvars, P. Yrjas and M. Hupa, *Fuel Processing Technology* **105**, 98 (2013).
7. J. Pettersson, C. Pettersson, H. Asteman, J. E. Svensson and L. G. Johansson, *Material Science Forum* **461–464**, 965 (2004).
8. J. Pettersson, H. Asteman, J. E. Svensson and L. G. Johansson, *Oxidation of Metals* **64**, 23 (2005).
9. S. Karlsson, J. Pettersson, L. G. Johansson and J. E. Svensson, *Oxidation of Metals* **78**, 83 (2012).
10. H. P. Nielsen, F. J. Frandsen, K. Dam-Johansen and L. L. Baxter, *Progress in Energy and Combustion Science* **26**, 283 (2000).
11. S. C. Cha and M. Spiegel, *Materials and Corrosion* **57**, 159 (2006).
12. Zahs, A., M. Spiegel, and H.J. Grabke, *Corrosion Science* **42**, 1093 (2000).
13. J. M. Abels and H. H. Strehblow, *Corrosion Science* **39**, 115 (1997).
14. H. J. Grabke, E. Reese and M. Spiegel, *Corrosion Science* **37**, 1023 (1995).
15. McNallan, M.J., W.W. Liang, S.H. Kim, and C.T. Kang, *Acceleration of the High Temperature Oxidation of Metals by Chlorine*, in *High Temperature Corrosion*, NACE, 316 (1983).
16. A. Zahs, M. Spiegel and H. J. Grabke, *Materials and Corrosion* **50**, 561 (1999).
17. Jonsson, T., T. Folkesson, J.E. Svensson, and L.G. Johansson, *An ESEM in situ investigation of initial stages of the KCl induced high temperature corrosion of a Fe-2.25Cr-1Mo steel at 400°C*. corrosion science, 2011. **53**, 2233 (2011).
18. Folkesson, N., T. Jonsson, M. Halvarsson, L.-G. Johansson, and J.-E. Svensson, *The influence of small amounts of KCl(s) on the high temperature corrosion of a Fe-2.25Cr-1Mo steel at 400 and 500°C*. *Materials and Corrosion*. **62** (2011).
19. P. Kofstad, *High Temperature Corrosion*, (Elsevier Applied Science, London, 1988).
20. S. Enestam, D. Bankiewicz, J. Tuiremo, K. Makela and M. Hupa, *Fuel* **104**, 294 (2013).
21. Y. Alipour and P. Henderson, *Corrosion Engineering Science and Technology* **50**, 355 (2015).
22. D. Bankiewicz, P. Vainikka, D. Lindberg, A. Frantsi, et al., *Fuel* **94**, 240 (2012).
23. E. Larsson, H. Gruber, K. Hellström, T. Jonsson, J. Liske and J. E. Svensson, *Oxidation of Metals* **87**, 779 (2017).
24. N. Folkesson, L. G. Johansson and J. E. Svensson, *Journal of the Electrochemical Society* **154**, C515 (2007).
25. P. Y. Hou, Y. Niu, T. J. Sum and J. Stringer, *Wear* **233–235**, 635 (1999).
26. K. Nakagawa and Y. Matunaga, *Materials at High Temperatures* **14**, 245 (1997).
27. K. Salmenoja, M. Hupa and R. Backman, *Journal of the Institute of Energy* **72**, 127 (1999).



28. Sato, Y., M. Hara, and Y. Shinata, *Effect of a small amount of HCl gas on high temperature oxidation of Fe-Cr alloys*. Proceedings of the International Conference on Surface Science and Engineering, Beijing, May 15–19, 1995, 395 (1995).
29. T. Jonsson, N. Folkesson, M. Halvarsson, J. E. Svensson and L. G. Johansson, *Oxidation of Metals* **81**, 575 (2014).
30. M. S. Pasten and M. Spiegel, *Materials and Corrosion-Werkstoffe Und Korrosion* **57**, 192 (2006).
31. Persdotter, A., E. Larsson, J. Liske, M.A. Olivas Ogaz, M. Sattari, and T. Jonsson, *Oxidation of Fe-2.25Cr-1Mo in presence of KCl(s) at 400°C - crack formation and its influence on oxidation kinetics*. Corrosion Science, In press. **CORSCI\_2019\_220**. <https://doi.org/10.1016/j.corsci.2019.108234>
32. Cantatore, V., M.A. Olivas Ogaz, J. Liske, T. Jonsson, J.-E. Svensson, L.-G. Johansson and I. Panas, *The Journal of Physical Chemistry C* **123**, 25957–25966 (2019).
33. Y. Joseph, G. Ketteler, C. Kuhrs, W. Ranke, W. Weiss and R. Schlogl, *Physical Chemistry Chemical Physics* **3**, 4141 (2001).
34. Muhler, M., R. Schlögl, and G. Ertl, *Journal of Catalysis* **138**, 413 (1992).
35. Dudley, G.J. and B.C.H. Steele, *Journal of Solid State Chemistry* **21**, 1 (1977).
36. S. Ito, N. Kubo, S. Nariki and N. Yoneda, *Journal of the American Ceramic Society* **70**, 874 (1987).
37. M. Muhler, J. Schütze, M. Wesemann, T. Rayment, et al., *Journal of Catalysis* **126**, 339 (1990).
38. Legutko, P., P. Stelmachowski, and A. Kotarba, *Promotion of iron-oxide with potassium as optimization of the soot combustion catalyst*. Challenges of Modern Technology, **3** (2012).
39. N. V. Dvoretiskii, E. G. Stepanov, T. N. Sudzilovskaya, G. R. Kotelnikov and V. V. Yun, *Inorganic Materials* **25**, 242 (1989).
40. A. Kotarba, I. Kruk and Z. Sojka, *Journal of Catalysis* **211**, 265 (2002).
41. L. Gmelin and R. J. Meyer, *Gmelin Handbook of Inorganic Chemistry*, Vol. 18, (Springer, Berlin, 1951).
42. Roine, A., *HSC Chemistry 7*. Outotec.

**Publisher's Note** Springer Nature remains neutral with regard to jurisdictional claims in published maps and institutional affiliations.